Hajiashrafi, T.; Salehi, S.; Kubicki, M.; Bauzá, A.; Frontera, A.; Flanagan, K. J.; Senge, M. O. (2019):
Solid-state supramolecular architectures of a series of Hg(ii) halide coordination compounds based on hydroxyl-substituted Schiff base ligands.
CrystEngComm 21, 6301–6312. doi: 10.1039/C9CE01078E

Solid-state Supramolecular Architectures of a Series of Hg(II) Halide Coordination Compounds Based on Hydroxyl-substituted Schiff Base Ligands

Taraneh Hajiashrafi,[a] Shiva Salehi,[a] Maciej Kubicki,[b] Antonio Bauzá,[c] Antonio Frontera,[c]*

Keith J. Flanagan,[d] Mathias O. Senge[d,e]

[a] *Department of Chemistry, Faculty of Physics and Chemistry, Alzahra University, PO Box 1993891176, Tehran, Iran*

[b] *Department of Chemistry, Adam Mickiewicz University, ul. Grunwaldzka 6, 60-780 Poznan, Poland*

[c] *Department of Chemistry, University of the Balearic Islands, Carretera de Valldemossa km 7.5, 07122 Palma de Mallorca, Illes Balears, Spain.*

[d] *School of Chemistry, SFI Tetrapyrrole Laboratory, Trinity Biomedical Science Institute, Trinity College Dublin, The University of Dublin, 152-160 Pearse Street, Dublin 2, Ireland*

[e] *Institute for Advanced Study (TUM-IAS), Lichtenberg-Str. 2a, 85748 Garching, Germany*

Abstract

Crystal engineering of coordination complexes has become an important research domain of modern inorganic chemistry. Herein, six Hg(II) coordination compounds containing 2-((pyridin-3-ylmethylene)amino)phenol and 4-((pyridin-4-ylmethylene)amino)phenol ligands were synthesized and characterized by single crystal X-ray crystallography and spectroscopic techniques. The crystal structure of these coordination compounds was studied using geometrical, Hirshfeld analyses as well as theoretical calculations. The results revealed the contribution of π-stacking, as well as hydrogen bonding interactions in the supramolecular architecture of these coordination compounds. This study may provide further insight into elucidating the role of weak non-covalent interactions on the supramolecular assembly of metal-containing compounds.

Introduction

Crystal engineering relies upon the understanding of intermolecular interactions and applying them for designing crystalline materials with desirable set of properties.[1, 2] Inorganic crystal engineering is the modelling, synthesis, and evaluation of the crystalline materials obtained from inorganic, organometallic, and bioinorganic building blocks.[3, 4] It is now well-known that the inherent properties of molecular crystal structures are rooted in the organization and relative orientation of constituent building blocks.[5] The results of the study in the field of inorganic crystal engineering revealed that the self-assembly of metal-containing species depends strongly on the structure of the organic ligands and their functionality which can provide a variety of complementary interactions such as hydrogen bonding,[6, 7] π-π staking,[8, 9] and halogen bonding[10, 11] between discrete sub-units. Thus, the rational design and selection of organic ligand is a crucial factor in the construction of inorganic solid-state structures.[12, 13] Beside the choice of the organic ligand, it was shown that different factors, such as the reaction conditions,[14-16] counter-ions,[17, 18] and the choice of metal ions,[19, 20] are also important in the construction of the final supramolecular architectures. In this regard, supramolecular chemists have designed a myriad of molecular scaffolds to clarify the inherent complexity of molecular self-association of inorganic and organometallic building blocks. These studies led to the discovery of several supramolecular synthons that can be used to design metallosupramolecular assemblies.[21-23]

In line with our research interest on studying the crystal structure of metal-containing compounds,[8, 24-27] a series of coordination complexes, namely $[Hg(L1)_2Cl_2]$ (**1**), $[Hg(L1)_2Br_2]$ (**2**), $[Hg(L1)_2I_2]$ (**3**), $[Hg(L2)_2Cl_2].H_2O$ (**4**), $[Hg(L2)_2Br_2]$.MeOH (**5**) and $[Hg(L2)_2I_2]$.MeOH (**6**), where **L1** is 2-((pyridin-3-ylmethylene)amino)phenol and **L2** is 4-((pyridin-4-ylmethylene)amino)phenol have been synthesized and characterized using single crystal X-ray diffraction and different spectroscopic methods. The crystal structure of these complexes were

studied using geometrical, Hirshfeld surface analyses, and theoretical calculations. This study has revealed the importance of hydrogen bonding as well as π-π stacking interactions in governing the supramolecular architecture of these series of coordination compounds.

Experimental Section

Materials and Apparatus

Chemicals and reagents were purchased from commercial sources. 2-hydroxybenzaldehyde, 2-methoxyaniline and anhydrous Hg(II) halides were purchased from Merck ® (Darmstadt, Germany) and used as supplied. The Schiff base ligands, 2-((pyridin-3-ylmethylene)amino)phenol (**L1**) and 4-((pyridin-4-ylmethylene)amino)phenol (**L2**), were prepared according to the previously reported method.[28] The infrared spectra were recorded on a Nicolet Fourier Transform IR, Nicolet 100 spectrometer in the range 500–4000 cm^{-1} using the KBr disk technique. Elemental analyses (carbon, hydrogen and nitrogen) were performed using an ECS 4010 CHN-O made in Costech, Italy. Melting points were measured by an Electrothermal 9100 melting point apparatus and corrected.

Single-Crystal Diffraction Studies

Single crystal X-ray diffraction data for **3** were collected on a Bruker APEX 2 DUO CCD diffractometer by using graphite-monochromated MoK_α (λ = 0.71073 Å) radiation. Handling of crystals followed procedures described before.[29] Crystals were mounted on a MiTeGen MicroMount and collected at 100(2) K by using an Oxford Cryosystems Cobra low-temperature device. Data were collected using omega and phi scans and were corrected for Lorentz and polarization effects by using the APEX software suite. Using Olex2, the structure was solved with the XT structure solution program, using the intrinsic phasing solution method and refined against $|F^2|$ with XL using least squares minimization.[30] Hydrogen atoms were generally placed in geometrically calculated positions and refined using a riding model. For all other

crystals, diffraction data were collected by the ω-scan technique at 100(1) K (**1**, **6**), 130(1) K (**4**, **5**) and at room temperature (**2**) on Rigaku XCalibur four-circle diffractometer with EOS CCD detector and graphite-monochromated MoK_α radiation (λ=0.71073 Å). The data were corrected for Lorentz-polarization as well as for absorption effects.[31] Precise unit-cell parameters were determined by a least-squares fit of the reflections of the highest intensity, chosen from the whole experiment. The structures were solved with SHELXT-2013 and refined with the full-matrix least-squares procedure on F^2 by SHELXL-2013. All non-hydrogen atoms were refined anisotropically, hydrogen atoms were placed in idealized positions and refined as 'riding model' with isotropic displacement parameters set at 1.2 times U_{eq} of appropriate carrier atoms. The crystals of **1** were found to be twinned, and this was taken into account both in data reduction and in structure refinement. The BASF factor[32] refined at 35.2(6)%. In **4** the hydrogen atom of the terminal hydroxyl group is disordered over two positions with s.o.f.'s of 50%. Interestingly, the atoms at these two alternative positions are involved in two different short hydrogen bonds, Details of data refinements can be found in Table 1 and further experimental and refinement detail can be found in the SI. CCDC-1939143 (for **1**), 1939144 (for **2**), 1937792 (for **3**), 1939145 (for **4**), 1939146 (for **5**), and 1939147 (for **6**) contains the supplementary crystallographic data for this paper. These data sets can be obtained free of charge from The Cambridge Crystallographic Data Centre via http://www.ccdc.cam.ac.uk/data_request/cif.

Computational methods

The energies of the complexes included in this study were evaluated at the PBE0-D3/def2-TZVP level of theory using the crystallographic coordinates. These calculationshave been carried out using the TURBOMOLE 7.3 program.[33] We have also used the Grimme's dispersion[34] correction since it is adequate for the evaluation of the non-covalent interactions described in this work. The basis set superposition error for the calculation of interaction energies has been corrected using the counterpoise method.[35] The NCI plot[36] iso-surfaces have

been used to characterize non-covalent interactions. They correspond to both favourable and unfavourable interactions, as differentiated by the sign of the second density Hessian eigenvalue and defined by the isosurface colour. The colour scheme is a red-yellow-green-blue scale with red for ρ^{+}_{cut} (repulsive) and blue for ρ^{-}_{cut} (attractive). Yellow and green isosurfaces correspond to weak repulsive and weak attractive interactions respectively.[37] The Gaussian-09[38] PBE-D/def2-TZVP wave function has been used to generate the NCI plot and the molecular electrostatic potential (MEP) surfaces using the 0.001 a.u. isosurface as a good estimation of the van der Waals surface and the surfaces have been visualized using the GaussView program.[38]

Synthesis of ligands L1 and L2

Ligands **L1** and **L2** were synthesized by mixing equimolar amounts of 2-hydroxy aniline (5 mmol) and 3-pyridinecarboxaldehyde (5 mmol) and 4-hydroxy aniline (5 mmol), and 4-pyridinecarboxaldehyde (5 mmol) in an ethanolic solution. The mixture was stirred for 15 min at 50°C, during which time a yellowish precipitate was formed. The yellowish precipitate was filtered off, washed with cold ethanol and dried in room temperature.

Ligand **L1**: IR (KBr pellet, cm^{-1}): 3378(br), 3061(w), 1895(w), 1625(s), 1578(s), 1483(vs), 1422(m), 1364(m), 1289(m), 1255(m), 1210(m), 1171(m), 968(m), 755(s), 703(m). Melting Point: 80-83°C.

Ligand **L2**: IR (KBr pellet, cm^{-1}): 3272(w), 3065(w), 2998(w), 2947(w), 2880(w),2804(w), 2737(w), 2677(w), 2603(w), 1575(vs), 1506(m), 1463(s), 1414(m), 1251(vs), 1155(vs), 1002(m), 840(s). Melting Point: 201-203°C.

Synthesis of coordination compounds $[Hg(L1)_2Cl_2]$ (1), $[Hg(L1)_2Br_2]$ (2), $[Hg(L1)_2I_2]$ (3), $[Hg(L2)_2Cl_2].H_2O$ (4), $[Hg(L2)_2Br_2].MeOH$ (5) and $[Hg(L2)_2I_2].MeOH$ (6)

To a solution of 0.1 mmol HgX_2 (X=Cl, Br, I) in 5 mL methanol, a solution of **L1** or **L2** (0.1 mmol) in 5 mL of methanol was added with stirring. The mixture was heated at 50˚C for about 30 minutes, followed by reduction of the solvent volume, resulting in the formation of a solid, bright yellow material. The precipitate was filtered, washed with cold methanol (3 × 2 mL), and

dried in a desiccator. The solid was recrystallized in boiling methanol, ethanol or acetonitrile (10 mL) and filtered. Upon slow evaporation of the filtrate at room temperature, colourless crystals of **1–6** suitable for X-ray diffraction were collected within a week.

*Compound **1** (yield 68%).* Anal. calcd for $C_{24}H_{22}Cl_2HgN_4O_3$: C, 42.02; H, 3.23; N, 8.17. Found: C, 41.9 H, 3.25; N, 8.12. IR (KBr pellet, cm^{-1}): 3313(w), 3028(w), 1614(w), 1577(vs), 1542(s), 1507(m), 1461(m), 1423(m), 1384(m), 1261(vs), 1163(m), 831(s), 542(v). Melting Point: 165–166°C (from CH_3CN).

*Compound **2** (yield 58%).* Anal. calcd for $C_{26}H_{28}Br_2HgN_4O_4$: C, 38.04; H, 3.44; N, 6.82. Found: C, 38.08 H, 3.42; N, 6.80. IR (KBr pellet, cm^{-1}): 3446(br), 3099(br), 2954(br), 2811(w), 2740(w), 2682(w), 2605(w), 1574(s), 1549(s), 1508(s), 1456(w), 1421(w), 1377(w), 1276(s),1237(s), 1164(m), 837(s). Melting Point: 192–193°C (from MeOH).

*Compound **3** (yield 62%).* Anal. calcd for $C_{26}H_{28}HgI_2N_4O_4$: C, 34.13; H, 3.08; N, 6.12. Found: C, 34.04 H, 3.02; N, 6.14. IR (KBr pellet, cm^{-1}): 3423(br), 3028(br), 2945(br), 2822(w), 2738(w), 2605(w), 1573(vs), 1541(m), 1509(m), 1457(m), 1418(m), 1374(m), 1284(s), 1237(vs),1158(s), 1008(s), 834(s). Melting Point: 173–174°C (from MeOH).

*Compound **4** (yield 46%).* Anal. calcd for $C_{24}H_{20}Cl_2HgN_4O_2$: C, 43.16; H, 3.02; N, 8.39. Found: C, 43.12 H, 3.10; N, 8.41. IR (KBr pellet, cm^{-1}): 3372(vs), 1706(w), 1626(w), 1588(s), 1484(vs), 1426(m), 1371(m), 1240(m), 1212(vs), 1028(w), 971(w), 799(vs), 748(vs), 694(s). Melting Point: 177–178°C (from EtOH).

*Compound **5** (yield 52%).* Anal. calcd for $C_{24}H_{20}Br_2HgN_4O_2$: C, 38.09; H, 2.66; N, 7.40. Found: C, 38.10 H, 2.62; N, 7.41. IR (KBr pellet, cm^{-1}): 3367(vs), 1626(s), 1587(s), 1484(vs), 1426(m), 1372(s), 1291(w), 1238(vs), 1212(vs), 1028(w), 971(w), 800(w), 747(vs), 640(s). Melting Point: 177–178°C (from EtOH).

*Compound **6** (yield 48%).* Anal. calcd for $C_{24}H_{20}HgI_2N_4O_2$: C, 33.88; H, 2.37; N, 6.58. Found: C, 33.78 H, 2.29; N, 6.50. IR (KBr pellet, cm^{-1}): 3360(vs), 1626(s), 1584(s), 1516(w), 1483(vs), 1425(m), 1516(vs), 1483(vs), 1425(w), 1371(s), 1290(w), 1240(w), 1037(w), 969(w), 800(vs), 745(vs), 692(s), 636(w). Melting Point: 152–153°C (from EtOH).

Results and Discussion

Synthesis and characterization

Cambridge Structural Database (CSD) revealed that ligand **L2** was previously utilized for the preparation of a number of coordination complexes.[39, 40] However, there are no crystal structures report using **L1** as a ligand for the formation of metal complexes. The six coordination complexes, $[Hg(L1)_2Cl_2]$ (**1**), $[Hg(L1)_2Br_2]$ (**2**), $[Hg(L1)_2I_2]$ (**3**),

$[Hg(L2)_2Cl_2]\cdot H_2O$ (**4**), $[Hg(L2)_2Br_2]\cdot MeOH$ (**5**) and $[Hg(L2)_2I_2]\cdot MeOH$ (**6**), figure 1, were synthesized by combining ligands **L1** or **L2** and M(II) halides in methanolic solution at 60°C and were crystallized from methanol, ethanol or acetonitrile in good yields. The coordination compounds were characterized using X-ray crystallography, FT-IR spectroscopy and Elemental analysis. ORTEP diagrams of **1**–**6** are drawn with 30% probability are shown in Figure S1 (supporting information).

Crystal structure analysis

Single crystal X-ray diffraction (SXRD) analyses revealed that compounds **1–3** are crystallized in the space groups $P2_1/c$ (**1** and **2**) and $P2_1/n$ (**3**) of the monoclinic system. The asymmetric units of **1–3** are identical and each consist of a Hg(II) ion, two coordinated **L1** ligands and two halide ions. In these compounds, the metal centre is coordinated by two pyridinic nitrogen atoms of two different **L1** ligands and two terminal halide ions. According to the four-coordinate geometry index (τ_4), defined by Houser and his co-workers,[41] the distorted tetrahedral geometry around Hg(II) ion can be better described as a seesaw structure, with a τ_4 value of 0.719, 0.714 and 0.701, for compound **1** to **3** respectively. Thus, the coordination geometry around Hg(II) in compound **3** is even more distorted from ideal tetrahedral than in compound **1**, due to the presence of a larger halide for a given metal ion. Selected bond distances and angles are listed in Table 2. In these three compounds, the *ortho*-hydroxy group interact intramolecularly with the imine nitrogen atom to form an O–H···N hydrogen bond. The directionality of the OH substituent with respect to the phenyl C–H bond provides a double hydrogen bond donor to the hydroxy group oxygen atom of a neighbouring molecular unit, Figure 1 and Figure 2.

In these three coordination compounds, the supramolecular architecture is constructed by linking neutral discrete coordination complexes through the synergistic O–H···O, C–H···X, and C–H···π hydrogen bonding interactions in the *ac*-plane, Figure 2, Table 3. In the structure

of compound **1**, the M–X···H contacts form a repeating head-to-head network through C5A–H5A···Cl1 (2.792(6) Å, 145.4(17)°) and head-to-tail network through C12B–H12B···Cl2 (2.858(6) Å, 138.8(14)° as seen in Figure S2. This is combined by an O–H···O interactions which are head-to-head in nature between O10B–H10B···O10B (2.251(18) Å, 140.2(7)° on one side of the molecule (Figure S3) and O10A–H10A···O10A (2.177(19) Å, 143.7(7)°. Additionally, the mononuclear units are stacked *via* C=N···π and weak Hg···π to form the three-dimensional supramolecular network, along the crystallographic *c*-axis (Figure S4). Combining these interaction profiles results in the crystal packing seen in Figure S5 with the layers of stacked molecular units separated by a Hg···Hg distance of 4.796(4) Å with a Cl–Hg–Cl angle of 149.4(2)°.

By altering the halogen substituent to a bromine atom (compound **2**) there are relatively few changes observed. The M–X···H contacts form a repeating head-to-head network through C5A–H5A···Br1 (3.029(15) Å, 134.0(9)°) and head-to-tail network through C12A–H12A···Br2 (3.079(14) Å, 145.9(10)° (Figure S6). However, as can be noted, rather than both ligands interacting (A and B ligands) in forming this network only the A-side is involved in these interactions due to the small rotation in the alignment of the molecular units when observed down the *a*-axis. The other notable differences are between the O–H···O interactions. Rather than the homo-interactions (A···A and B···B), a hetero-network is now present (A···B) between the hydroxy groups as seen in Figure S7 (O10B–H10B···O10A (2.397(10) Å, 123.5(8)°)) and (O10A–H10A···O10B (2.317(10) Å, 141.3(7)°)). Similar to compound **1** the mononuclear units are stacked *via* C=N···π and weak Hg···π interactions. Due to the changing the halogen atom type, there is a minor increase in the Hg···Hg separation of 4.931(14) Å and a Br–Hg–Br angle of 148.1(5)° (Figure S8). This results in a slightly looser packing than compound **1**, however, the relative patterns are the same (Figure S9).

In the structure of compound **3**, the molecular arrangement is a mix between both compound **1** and **2**. The M–X···H contacts is seen through the head-to-head interaction [C12B–H12B···I2 (3.132(1) Å, 141.2(2)°)] and the head-to-tail interaction [C5B–H5B···I1 (3.087(1) Å, 135.0(3)°)] which is similar to compound **1** with contacts exclusively on the B ligand (Figure S10). The O–H···O interactions are more similar to compound **2** with the A···B pattern (O10B–H10B···O10A (2.230(4) Å, 142.0(5)°)) and (O10A–H10A···O10B (2.070(5) Å, 152.0(5)°) (Figure S11). As with compounds **1** and **2**, the mononuclear units are stacked *via* C=N···π and weak Hg···π interactions with a Hg···Hg separation is 4.913(3) Å and an I–Hg–I angle of 149.4(12)° (Figure S12) and combined with the interactions stated, result in the crystal packing seen in Figure S13.

Hirshfeld surface analysis is a three-dimensional graphical tool which helps one understand the intermolecular contacts present in the crystal structure.[42] The contribution percentages of different interactions to the Hirshfeld surface areas are shown in Figure 5. Hirshfeld Surface analysis revealed that the H···H interactions are dominant in compounds **1** to **3**. Additionally, the introduction of a larger halide species to the Hg(II) metal ion results in the contribution of M–X···H hydrogen contacts increases (from 16.3 to 17.3 and then to 18.8, respectively), while the contribution of C=N···π (from 7.0 to 5.8 and then to 5.7, respectively) as well as π···π (from 5.5 to 4.6 and then to 4.4, respectively) decreases.

Compound **4** is crystallized in space group *I*2/*a* of the Monoclinic system, while compounds **5** and **6** in the *Pba*2 of the Orthorhombic system. The asymmetric units of compounds **4–6** contain half of the Hg(II) ion, a coordinated **L2** ligand, a halide ion, as well as uncoordinated solvent (H_2O in the case of compound **4** and CH_3OH in the cases of **5** and **6**) molecule.

SXRD revealed that compound **4** is a 1D coordination polymer built up from chloride-bridged Hg(II) edge-sharing octahedral extending along the crystallographic *b*-axis, Figure 3. In this

compound, the Hg(II) ion is in a distorted octahedral geometry with an N_2Cl_4 donor set provided by the four bridging chloride ions in the basal plane and two pyridine nitrogen atoms from two **L2** ligands in the apical position, Table 2. The intra-chain metal···metal separation is 3.844 Å and the Hg···Hg···Hg intra-chain angle is 180˚ which is at the upper limit weak mercurophilic interactions.[43 44]

The infinite 1D coordination polymer chain is further stabilized by weak intra-chain π···π stacking interactions with ring centroid-to-centroid distances of 3.844 Å, Table 4. As depicted in Fig. 3, the overall supramolecular structure of compound **4** results from the association of neighbouring coordination polymer chains *via* a set of non-classical C_{py}–H···Cl–Hg, $_{phen}$C–H···π hydrogen bonding interactions in the *ac*-plane, Table 3. Also, the water molecule of crystallization links the polymeric chains through $_{water}$O–H···O–H_{phen} and $_{imine}$C=N···H–O_{water} hydrogen bonding interactions (Figure S14). Additionally, there is the presence of an O–H···O interaction between the phenol moieties (Figure S15) which forms a continuous rod-like hydrogen bonded network between individual molecular units. These interactions above combine to form the crystal packing seen in Figure S16.

In compounds **5** and **6**, the Hg(II) ion is four-coordinated in a seesaw geometry with two pyridinic nitrogen atoms of two different **L2** ligands at the pivot position and two terminal halide ions at the plank and τ_4 values of 0.72 and 0.70, respectively. In comparison with compounds **1–3**, the hydroxy group of ligand **L2** in compounds **4–6** is more accessible for intermolecular hydrogen bonding contacts, as there is no possibility for intramolecular O–H···N_{imine} hydrogen bonding. Discrete neutral $[HgX_2(L2)_2]$ units stacked on one another *via* a combination of weak C–H···X (3.178(2) Å for **5** and 3.282(1) for **6**), $_{imine}$C=N···π (N···ring-centroid= 3.445(5) Å for **5** and 3.444(2) Å for **6**) and C–H···π (C–H···ring-centroid= 3.542(1) Å for **5** and 3.701(1) Å for **6**) interactions, along the *c*-direction, Figure 4, Table 3, and Table 4. The overall supramolecular architecture of compounds **5** and **6** is constructed by linking

discrete coordination complexes via $_{imine}$C–H···I–Hg, $_{phen}$O–H···O$_{MeOH}$ and O–H···N$_{imine}$ hydrogen bonds in the *ab*-plane, Figure 4. These interactions change the type of packing observed in compounds **5** and **6** to be an arrow-like stacking motif (Figure S17 and S18) as apposed to the rod-like motif seen in compound **4**. By looking at Figure S19 (**5**) and S20 (**6**) it is clear the methanol solvate plays a major role in complexing the individual molecular units to form an almost orthogonal orientation hydrogen bonded network in the crystal lattice. In contrast to compound **3** where a water molecule is included in the crystal lattice resulting in the parallel alignment of molecules. However, the almost co-planar alignment between ligands is a much larger driving force for this arrangement. Combining these features results in the wave-like pattern observed in Figure S21 (**5**) and S22 (**6**).

Hirshfeld surface analysis of compounds **5** and **6** also revealed that upon the increase of the size of halide ion, the contribution of M–X···H hydrogen contacts increases (17.0 to 17.8%, respectively), while that of C–H···π (9.8 to 9.4%, respectively) and C=N···π (9.8 to 9.4%, respectively) decreases, Figure 5.

Compared to the structures of other HgX_2L complexes previously reported in the literature, such as where L = 3,4-pyridinedicarboxamides (Rana *et al.*) or L = (*E*)-*N*-(pyridin-2-ylmethylidene)arylamines (Baul *et al.*) we are presented with a rather unique case.[x1, x2] Of the structures herein, it is apparent that forming coordinate polymers is less likely, with only compound **4** achieving this, rather the X···H hydrogen contacts and π-interactions are a dominant feature. This feature is rather similar to our previous studies on $M(II)L_2X_2$ compounds.[8] Compared to the work by Rana *et al.*, the different use of ligands has profound changes on the types of networks formed. The for complexes where L = 3,4-pyridinedicarboxamides, the relatively small nature of the associated ligands and the flexibility of the functional groups leads to an increase in the potential to form large repeating networks and a multitude of coordinate polymers from through simple changes in the backbone of

pyridinedicarboxamides. While our case provides a more rigid scaffold with limited functional groups which allows us to focus on the contribution of π-stacking, as well as hydrogen bonding interactions in the formation of supramolecular arrays specifically. Compared to the works of Baul *et al*., we saw an alternate shift if perspective by alternating the nitrogen of the pyridine moiety the potential to form a HgX_2L motif is eliminated resulting exclusively in the HgX_2L_2 complexes. Due to the space occupied by the inclusion of a second ligand, the formation of dimers or polymers metallo-halide interactions is all but eliminated. This is why in essences compound **4** is an anomaly in this series by its preference to from a coordinate polymer. There are two main differences that can be expressed in this case when comparing compound **4** to either **5** or **6**. The first one is the simple fact that either due to the higher charge density and lower ionic size of chlorine compared to either bromine or iodine allows the ligands to occupy an orientation (~180° for N–Hg–N). The second differences that the Cl–Hg bond in compound **4** is more in ionic in character with an X–M distances much larger than that of compound **1** and even greater than that of compound **6** (see Table 2). Finally, compared to compound **1**, it is clear that no favourable conformation for **L1** to occupy that would potentially result in the same coordinate polymer complex as compound **4**.

Theoretical Study

The theoretical study is devoted to the analysis of the intermolecular π-interactions that govern the formation of supramolecular 1D columns in compounds **1–6** as described below, Figure 1. Initially, we computed the molecular electrostatic potential (MEP) plotted onto the approximate van der Waals surface (isosurface 0.001 a.u.) in order to investigate the electron rich and electron poor region of the molecule. We have selected compounds **1** and **5** as representative examples. The MEP surfaces are represented in Figure 6. It can be observed that the most positive region is located at the hydrogens of the OH substituents, which exhibit MEP values of +36 and +54 kcal/mol, for **1** and **5**, respectively. The smaller value observed for **1** is likely

due to the formation of an intramolecular OH···N H-bond that decreases the acidity of the phenolic hydrogen. The most negative region is located at the Cl or Br ligands, as expected. The MEP value is also negative at the phenolic O-atom (–23 kcal/mol). This analysis indicates that the most favoured interaction from an electrostatic point of view should be a H-bond between the Ar–OH and the halide ion. However, in the solid state, these OH groups establish H-bonds with either solvent molecules (MeOH) or with the phenolic O-atom, thus preventing the formation of OH···X interactions. Moreover, the inspection of the MEP surfaces also reveals that the MEP above the aromatic ring is either slightly positive or negative thus adequate for establishing π-interactions dominated by dispersion rather than electrostatic effects.

Figure 7a shows partial views of the X-ray of structures of compounds **1**, **2** and **3** (H-atoms omitted), which are very similar, and all exhibit the formation of infinite 1D supramolecular columns. These supramolecular columns are formed by the propagation of the HgL_2X_2 complexes along the *a*-axis of the crystal by means of π···π interactions. In Figure 7b, one representative dimer has been shown, extracted from the supramolecular chain of compound **2**. A close examination of the dimer reveals that the halides are close to the π-system of the Hg-coordinated pyridine ring, which agrees well with the MEP analysis (see Figure 6) that shows that the MEP value over this ring is positive (+8.4 kcal/mol). Moreover, the N-atom of the imidic group is located over the π-system of the non-coordinated ring. We have evaluated the influence of the halide on the dimerization energy, and it can be observed that it is almost negligible. That is, all compounds present similar interaction energies (within the accuracy of the method) ranging from –35.8 to –34.2 kcal/mol and similar to the geometric features regarding X···π and N···π distances (denoted as d1 and d2, respectively in Figure 7b). The interaction is very strong due to the large overlap of the π-systems and the X···π interactions. In order to further characterize the non-covalent interactions, we have used the NCI plot index computational tool. Non-covalent interactions are efficiently visualized and identified by using

the NCI plot index. It allows an easy assessment of host-guest complementarity and the extent to which weak interactions stabilize a complex. Figure 7c shows the NCI plot obtained for the dimer extracted from the infinite 1D column in compound **2**. It can be observed the presence of very extended green isosurface that embraces the whole region between both molecules. Therefore, the complementary between both molecules is excellent, since practically the whole conjugated π-system of the ligand and the HgX_2 moiety participate in the binding. This strongly agrees with the large interaction energies commented above. The NCI plot confirms the X···π interaction and also reveals that the halide ligands also interact attractively with the Hg(II) metal centre (denoted as Hg···X).

Figure 8a shows partial views of the X-ray of structures of compounds **5** and **6** (H-atoms omitted). Compound **4** has not been included in this study due to its polymeric nature. Both compounds **5** and **6** exhibit the formation of infinite 1D supramolecular columns. These supramolecular columns are formed by the propagation of the HgL_2X_2 complexes along the *c* axis of the crystal by means of π···π interactions. In Figure 8b, one representative dimer has been shown, extracted from the infinite 1D columns. A close examination of the dimer reveals that each halide is close to one C-atom of the Hg-coordinated pyridine ring. Moreover, the C-atom of the imidic group (instead of the N-atom observed in complexes **1**–**3**) is located over the π-system of the non-coordinated ring. Both compounds present equivalent interaction energies and geometric features thus indicating that the type of halide used has a very small influence of the assembly. The interaction is also strong but weaker compared to the other series of complexes (see Figure 7b). A likely explanation is that the X···π interaction is weaker in this series of complexes because the MEP over the coordinated pyridine is significantly smaller in compound **4** (+1.2 kcal/mol) than in compound **1** (see Figure 6). We have also used the NCI plot index computational tool to assess the host-guest complementarity and the extent to which weak interactions stabilize this dimer. Figure 8c shows the NCI plot of the dimer of compound

5 and it can be observed that the presence of very extended green isosurfaces thus showing a high complementary. A smaller isosurface is located between both HgX_2 moieties that are characteristic of the Hg···X interaction.

Conclusion

Herein, six new coordination complexes of Hg(II) have been successfully synthesized and characterized using single crystal X-ray diffraction analysis and spectroscopic methods. The crystal structures of these compounds are the subject of geometrical and statistical analyses as well as theoretical calculations. Stacking interactions involving the organic ligands in the crystal structure result in 1D infinite supramolecular columns for all discrete compounds. We have used the molecular DFT calculations and evaluated energetically the strength of these contacts in these compounds. In addition to the formation of π-stacking interactions, the HgX_2 moiety also participates in the reinforcement of the supramolecular assembly as shown by the NCI plot index.

AUTHOR INFORMATION

Corresponding Authors

Phone: +98-21-85692619

E-mail: t.hajiashrafi@alzahra.ac.ir (T.Hajiashrafi)

ACKNOWLEDGMENT

We gratefully acknowledge the financial support from the Research Council of Alzahra University. AF and AB thank the MINECO/AEI of spain (project CTQ2017-85821-R, FEDER funds) for financial support. MOS acknowledges funding from Science Foundation Ireland (SFI IvP IvP 13/IA/1894) and through an August-Wilhelm Scheer Gastprofessor award (TU Munich). We thank the “Centre de Tecnologies de la Informació” (CTI) at the UIB for computational facilities.

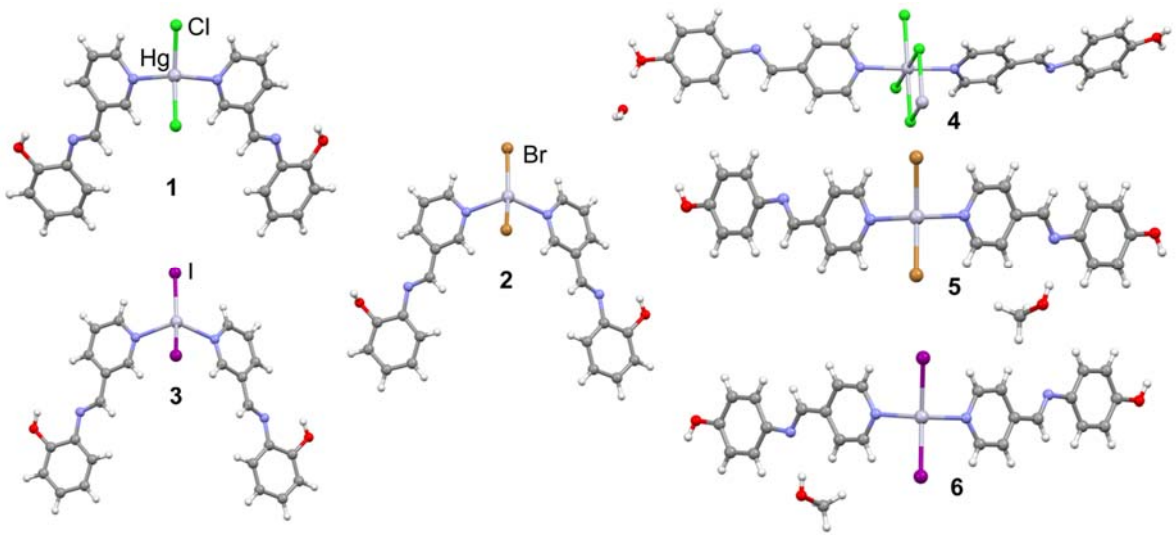

Figure 1. Molecular structure of the coordination compounds **1–6** showing the coordination geometry around the Hg(II) ion.

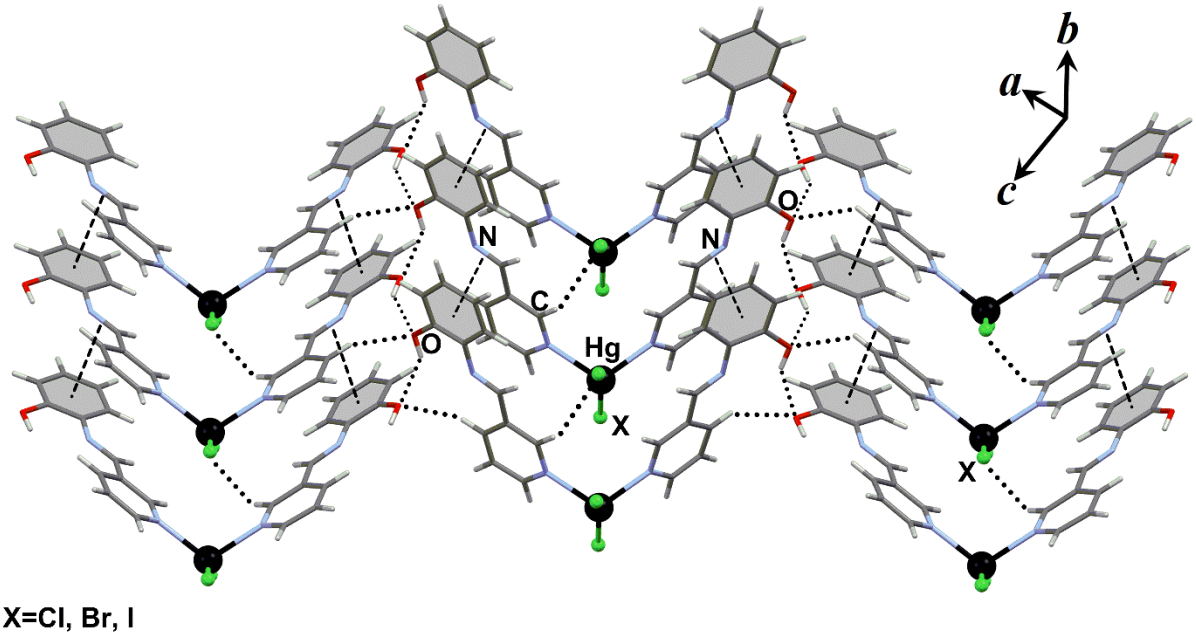

Figure 2. Representation of the self-assembly of compounds **1-3** showing the association of discrete molecular units through C–N···π interactions in the crystallographic *c*-direction and O–H···O, C–H···Cl and C–H···π hydrogen bonding interactions in the *ac*-plane.

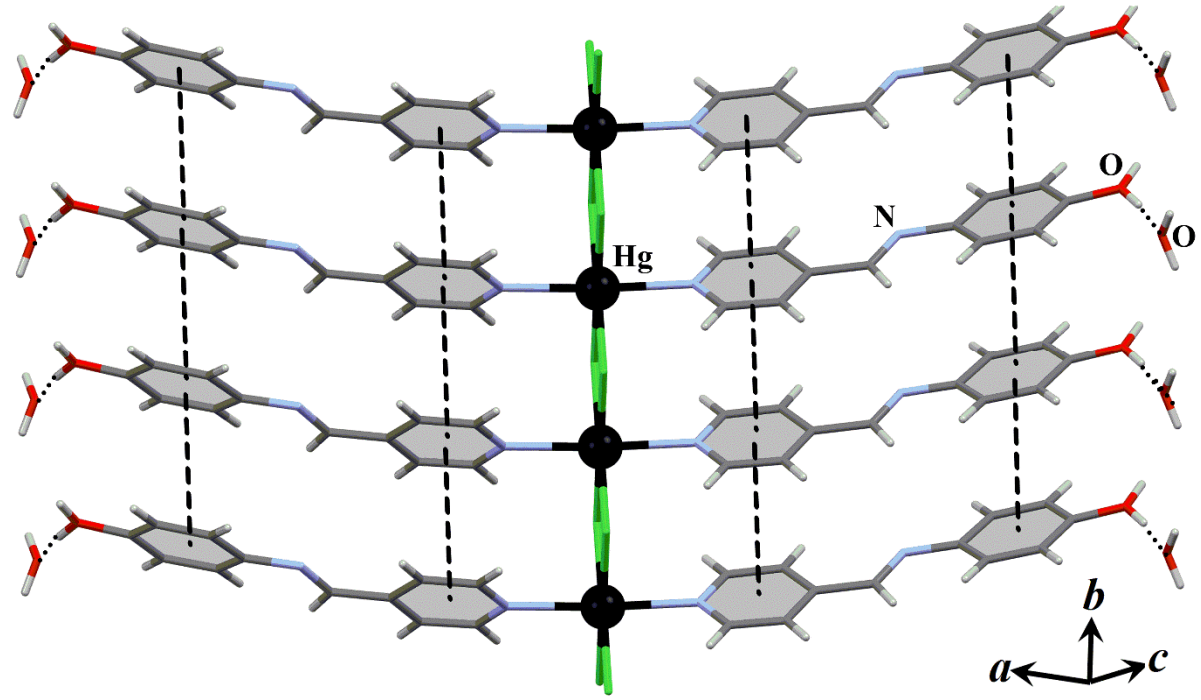

Figure 3. An infinite 1D coordination polymer chain of compound **4,** along the crystallographic *b*-axis, which is further stabilized by weak intra-chain π···π stacking interactions. The water molecules of crystallization link the polymeric chains through $_{water}$O–H···O–H$_{phen}$ hydrogen bonding interactions.

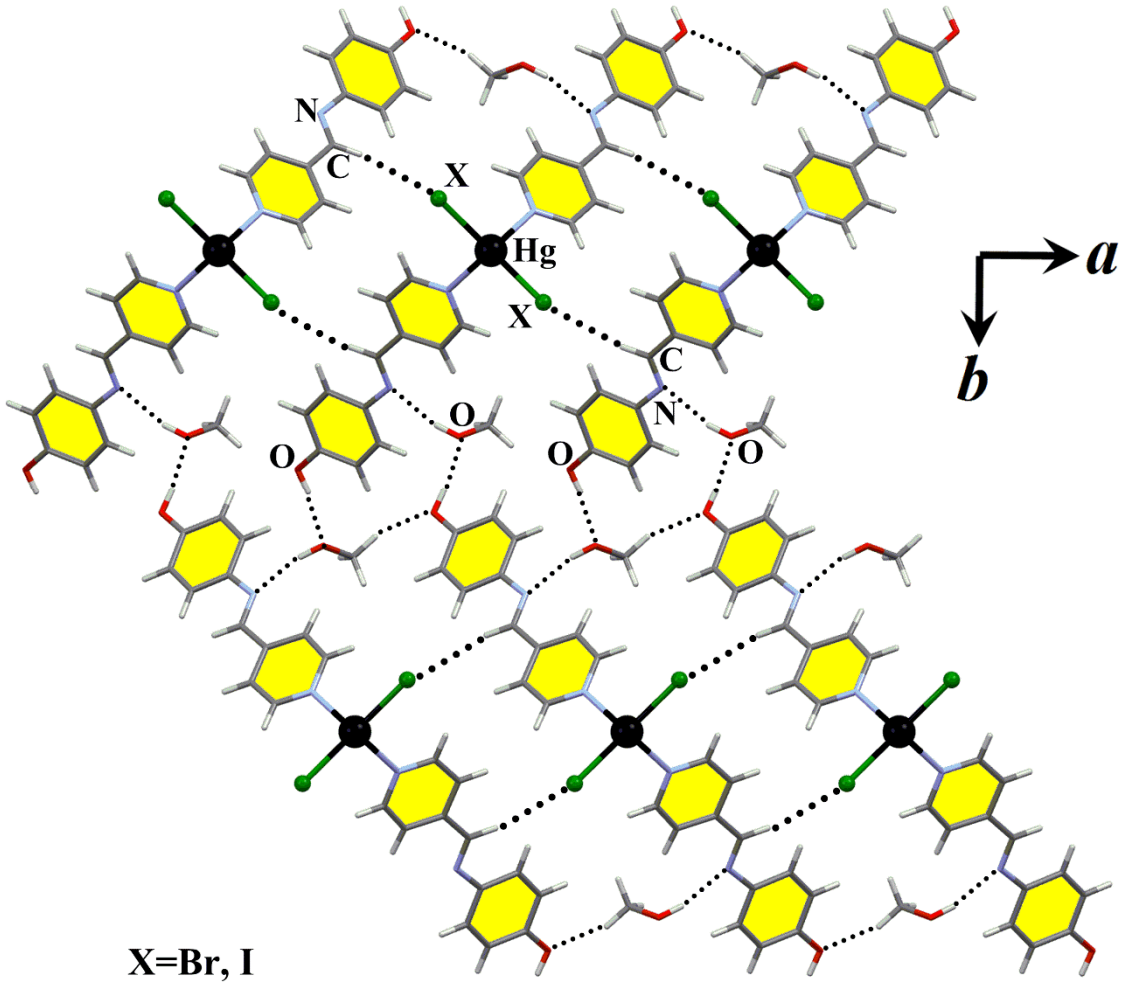

Figure 4. The overall supramolecular architecture of compounds **5** and **6** is constructed by linking discrete coordination complexes $[HgX_2(L2)_2]$ via $_{imine}C–H\cdots X–Hg$, $_{phen}O–H\cdots O_{MeOH}$ and $O–H\cdots N_{imine}$ hydrogen bonds in the *ab*-plane.

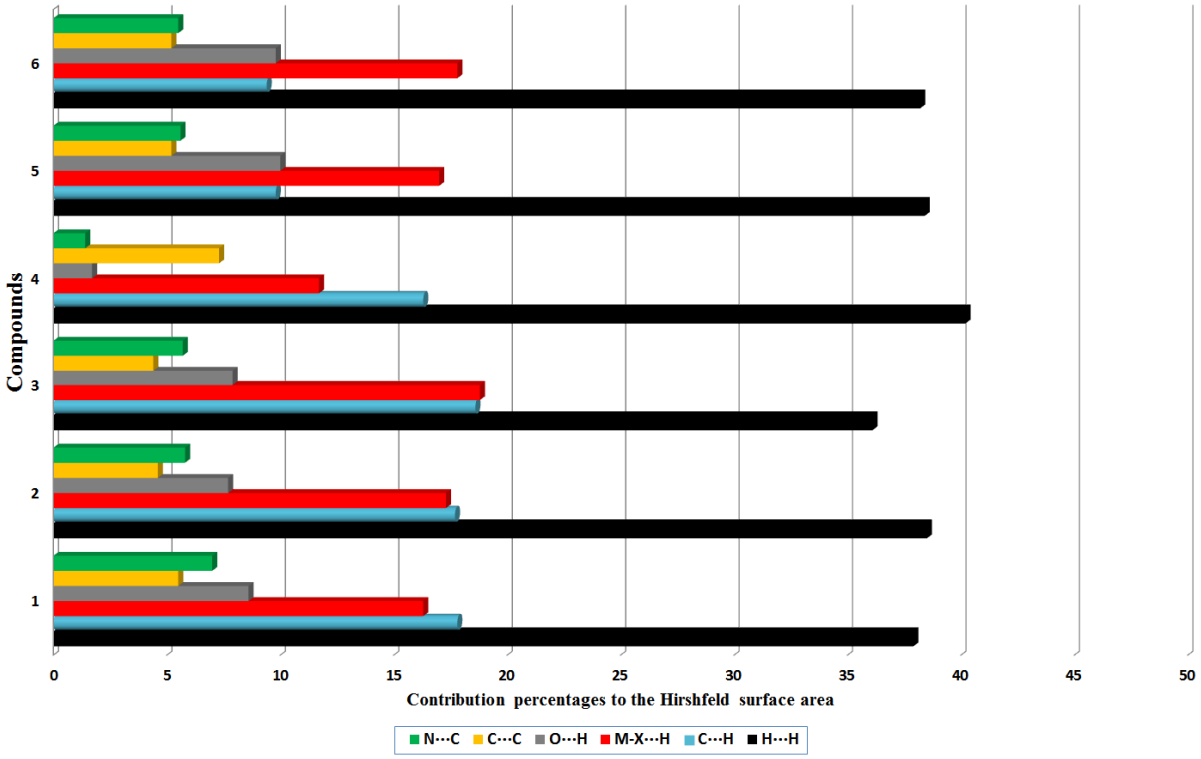

Figure 5. Relative contributions of various non-covalent contacts to the Hirshfeld surface area in complexes **1**–**6**.

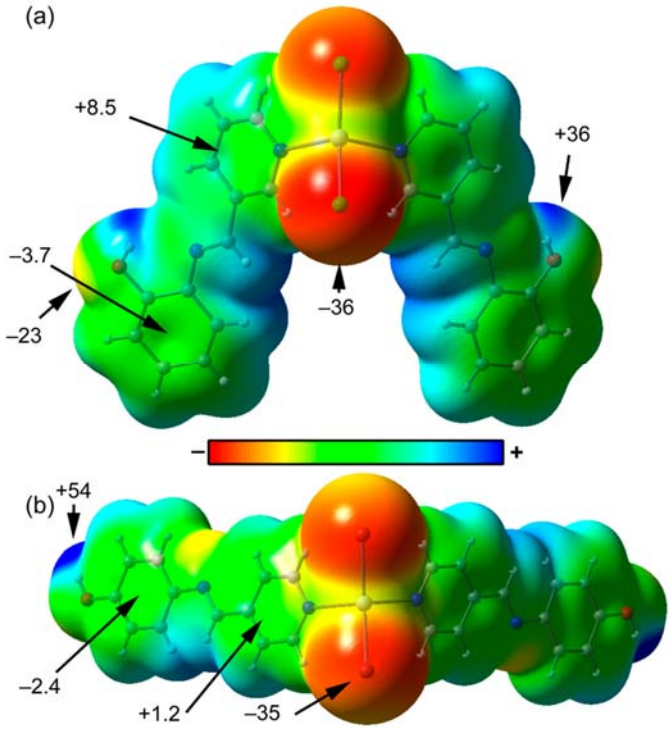

Figure 6 MEP surfaces of compounds **1** (a) and **3** (b) (isosurface 0.001 a.u.) at the PBE0/def2-TZVP level of theory. The values at selected points of the surface are indicated in kcal/mol. Å

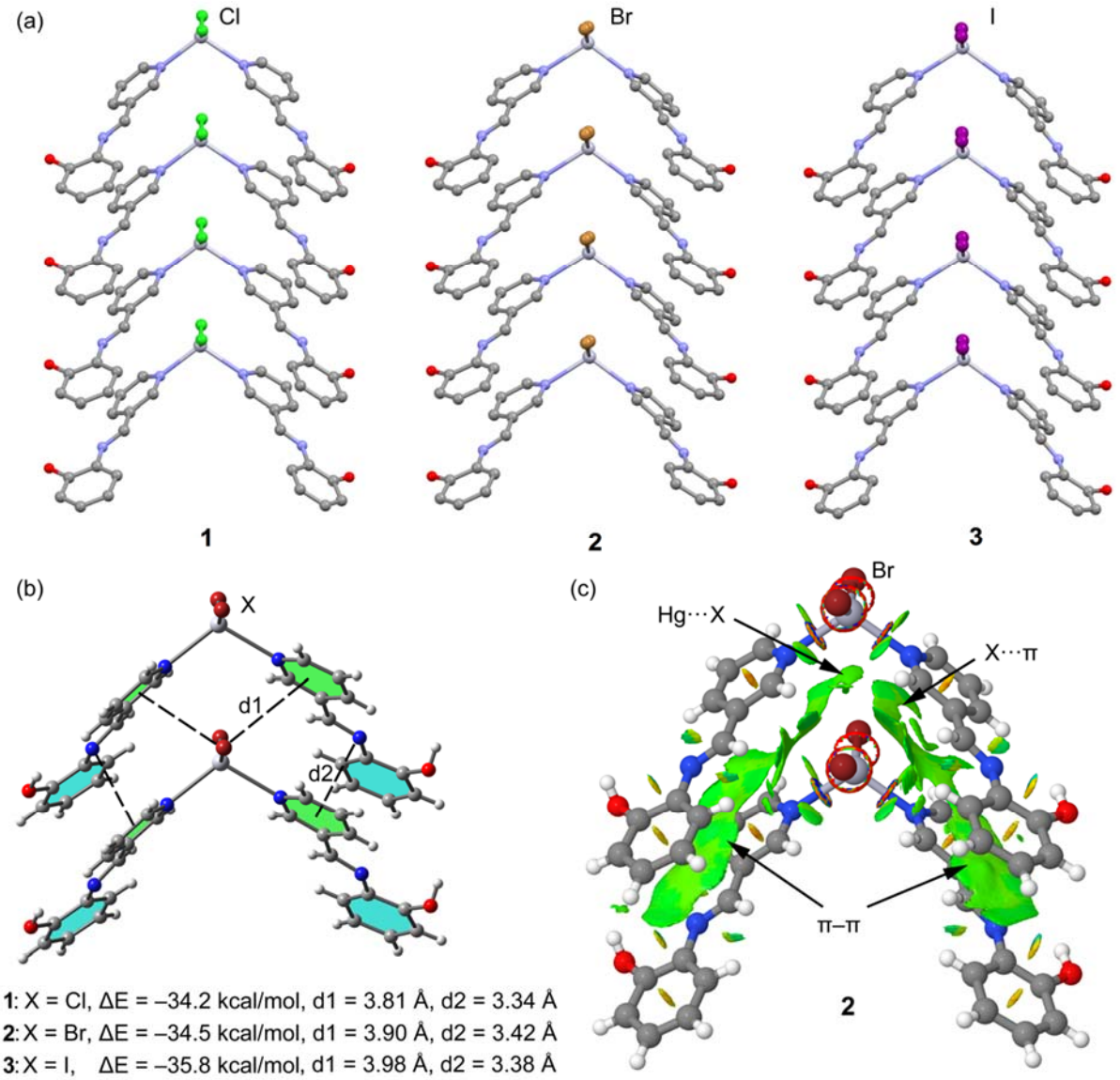

Figure 7 (**a**) Partial view of the X-ray structures of compound **1**, **2**, and **3**. H-atoms omitted for clarity. (**b**) Theoretical models used to evaluate the non-covalent interactions. **(c)** NCI plot of the self-assembled dimer in **2**, as a representative model. The gradient cut-off is $s = 0.35$ a.u., and the colour scale is $-0.04 < \rho < 0.04$ a.u.

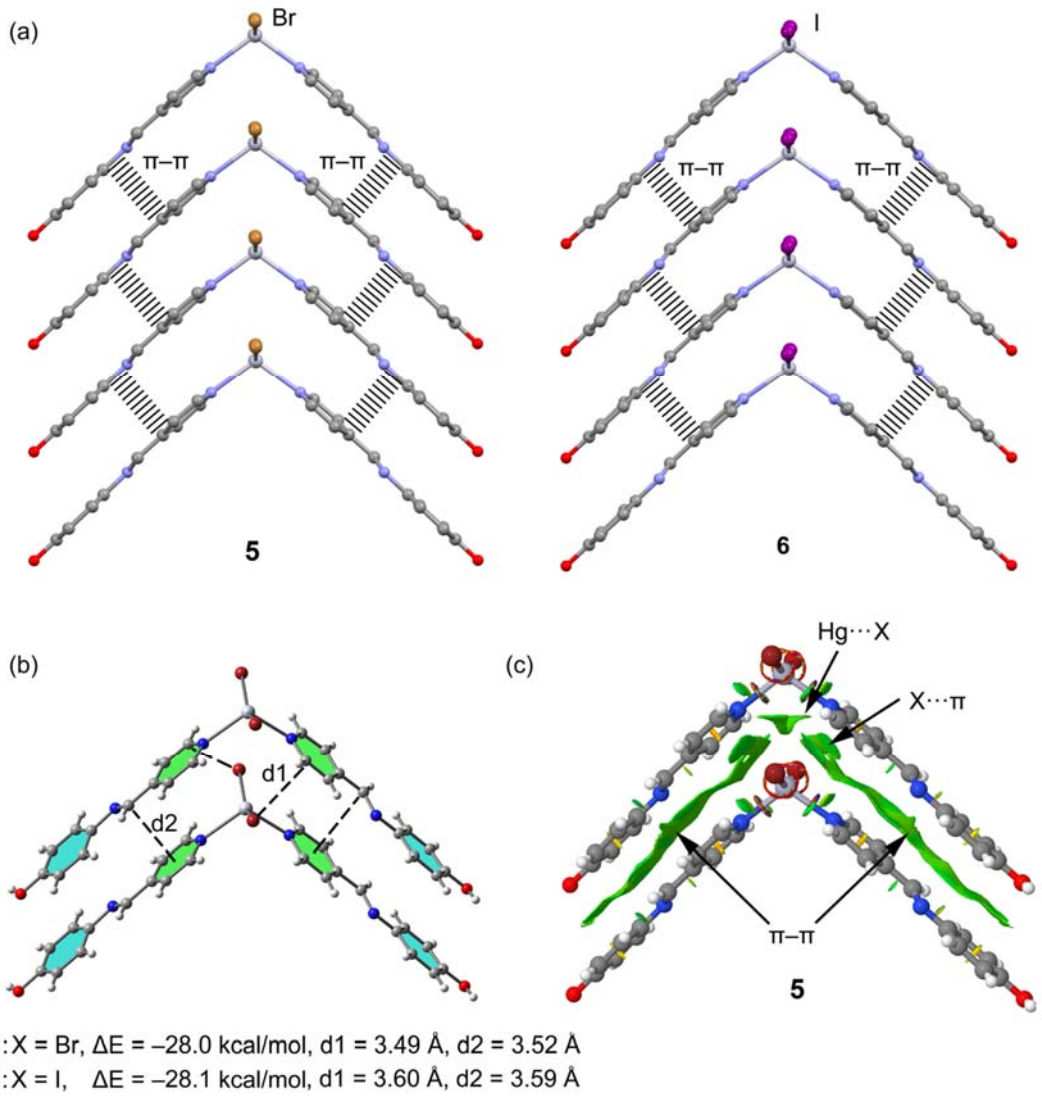

Figure 8 (**a**) Partial view of the X-ray structures of compound **5** and **6**. H-atoms omitted for clarity. (**b**) Theoretical models used to evaluate the non-covalent interactions. **(c)** NCI plot of the self-assembled dimer in **5**, as a representative model. The gradient cut-off is $s = 0.35$ a.u., and the colour scale is $-0.04 < \rho < 0.04$ a.u.

Table 1. Structural data and refinement for compounds **1-6**

Complex	**1**	**2**	**3**	**4**	**5**	**6**
formula	$C_{24}H_{20}Cl_2HgN_4O_2$	$C_{24}H_{20}Br_2HgN_4O_2$	$C_{24}H_{20}HgI_2N4O_2$	$C_{24}H_{22}Cl_2HgN_4O_3$	$C_{26}H_{28}Br_2HgN_4O_4$	$C_{26}H_{28}HgI_2N_4O_4$
fw	667.93	756.85	850.83	685.95	820.93	914.91
λ/Å	0.71073	0.71073	0.71073	0.71073	0.71073	0.71073
T/K	100(1)	298(2)	100(2)	130(1)	130(1)	100(1)
crystal system	monoclinic	monoclinic	monoclinic	monoclinic	orthorhombic	orthorhombic
space group	$P2_1/c$	$P2_1/c$	$P2_1/n$	$I2/a$	$Pba2$	$Pba2$
a/Å	19.6861(19)	4.93100(14)	4.9128(3)	17.5323(6)	8.9742(2)	9.1791(6)
b/Å	4.7958(4)	17.3546(4)	17.8054(10)	3.84380(10)	31.8029(8)	32.206(2)
c/Å	25.169(2)	28.8630(8)	28.6882(16)	34.5553(10)	4.70330(14)	4.7036(3)
α/°	90	90	90	90	90	90
β/°	101.404(9)	91.909(2)	91.1330(10)	100.079(3)	90	90
γ/°	90	90	90	90	90	90
$V/Å^3$	2329.3(4)	2468.60(11)	2509.0(3)	2292.77(12)	1342.35(6)	1390.49(15)
$D_{calc}/g.m^{-3}$	1.905	2.036	2.185	1.987	2.027	2.185
Z	4	4	4	4	2	2
$\mu\ (mm^{-1})$	6.867	9.500	2.252	6.982	8.733	7.794
F(000)	1288.0	1432.0	1576.0	1328.0	788.0	860.0
2θ (°)	5.852 to 50	6.324 to 49.994	3.646 to 54.36	7.186 to 53.196	6.846 to 53.026	5.84 to 56.568
R (int)	0.0405	0.0605	0.0602	0.0489	0.0252	0.0772
GOOF	1.066	1.361	1.128	1.128	1.077	1.109
$R_1a(I>2\sigma(I))$	0.0980	0.0833	0.0299	0.0223	0.0383	0.0451
$wR_2b(I>2\sigma(I))$	0.2655	0.1248	0.0429	0.0559	0.0970	0.0985
ccdc number	1939143	1939144	1937792	1939145	1939146	1939147

[a] $R_1 = \Sigma||F_o| - |F_c||/\Sigma|F_o|$. [b] $wR_2 = [\Sigma(w(F_o^2 - F_c^2)^2)/\Sigma w(F_o^2)2]^{½}$.

Table 2. Selected bond distances (Å) and angles (°) for compounds **1**-**6**.

	Compounds						
		1	**2**	**3**	**4**	**5**	**6**
Bond distance	Hg1–N1	2.350(18)	2.390(9)	2.407(4)	2.332(4)	2.398(14)	2.419(11)
	Hg1–X1 (X1=N1B for **1–3**)	2.379(17)	2.423(9)	2.451(3)	2.7147(8)	2.5120(17)	2.6760(8)
	Hg1–X1[1]	2.363(6)	2.4796(14)	2.6557(3)	2.7146(8)	2.5121(17)	2.6759(8)
	Hg1–X1[2]	2.407(6)	2.5162(14)	2.6857(4)	2.7280(8)	-	-
	Hg1–X1[3]	-	-	-	2.7281(8)	-	-
Bond angle	N1–Hg1–N1[1]	102.8(5)	102.7(2)	-	176.99(10)	107.8(4)	110.5(5)
	N1–Hg1–X1[1]	109.1(6)	111.1(3)	-	91.34(7)	96.7(2)	99.7(2)
	N1[1]–Hg1–X1[1]	100.4(4)	98.4(2)	101.56(8)	90.78(7)	100.7(2)	-
	X1[1]–Hg1–X1	97.2(4)	98.5(2)	-	90.43(3)	150.29(8)	149.73(5)
	N1–Hg1–X1[2]	149.4(2)	148.10(6)	149.389(12)	88.66(7)	-	-
	N1[1]–Hg1–X1[2]	94.2 (5)	95.9(2)	98.18(18)	89.21(7)	-	-
	X1–Hg1–X1[3]	-	-	111.76(11)	179.717(18)	-	-
	X1[1]–Hg1–X1[3]	-	-	96.53(8)	89.86(3)	-	-
	X1–Hg1–X1[2]	-	-	97.58(8)	89.86(3)	-	-
	N1–Hg1–X1	102.8(5)	102.7(2)	-	-	-	97.4(2)
	N1[1]–Hg1–X1	109.1(6)	111.1(3)	-	-	-	99.7(2)

Sym.Codes. for compound **1,2** and **3:** [1,2]=x,y,z, for compound **4:** [1]= 1/2-x,+y,1-z; [2] =+x,1+y,+z; [3] =1/2-x,1+y,1-z compound **5** and **6:** [N!B]=1-x, 1-y, z; **[1]**= -x, 1-y, z

Table 3. Selected hydrogen bond geometries for coordination compounds **1-6**.

Compound	D-H…A	d(D-H)/Å	d(H…A)/Å	d(D…A)/Å	<D-H…A/°	Sym. Code
1	C12B–H12B···Cl2	0.95(2)	2.858(6)	3.63(3)	138.8(4)	1-x, 2-y,1-z
	C2B–H2B···Cl2	0.92(2)	2.943(6)	3.65(2)	132.5(12)	x, -1+y ,2
	C5A–H5A···Cl1	0.95(3)	2. 792(6)	3.61(3)	145.4(17)	-x, -y, 1-z
	O10A–H10A···N8A	0.841(19)	2.209(15)	2.67(2)	114.8(12)	x, y, z
	O10A–H10A···O10A	0.841(19)	2.177(19)	2.90(2)	143.7(7)	-x, -1/2+y,1/2-z
	O10B–H10B···N8B	0.839(18)	2.189(15)	2.65(2)	114.7(11)	x, y, z
	O10B–H10B···O10B	0.839(18)	2.251(18)	2.946(19)	140.2(1)	1-x, -1/2+y,3/2-z
	C4B–H4B···O10B	0.95(2)	3.271(17)	3.50(3)	95.8(16)	x,-1+ y, +z
2	C4B–H4B···O10A	0.93	2.52	3.379	153.32	x, y, z
	C4A–H4A···O10B	0.93	2.57	3.305	135.30	-1/2+x,3/2-y,+z
	O10B–H10B···O10A	0.82	2.39	2.930	123.48	x, y, z
	O10A–H10A···O10B	0.82	2.31	3.00	141.26	1/2+x,3/2-y,**1**+z
3	C4B–H4B···O10A	0.950(5)	2.603(3)	3.294(6)	129.9(3)	-1/2+x,1/2-y,-1/2+z
	C4A–H4A···O10B	0.949(4)	2.438(3)	3.296(6)	150.3(3)	-1/2+x,1/2- y,1/2+z

	O10B–H10B···O10A	0.856(4)	2.23(4)	2.953(5)	142(5)	-1/2+ x, +1/2-y, -1/2+ z
	O10A–H10A···O10B	0.85(4)	2.07(5)	2.854(5)	152(5)	-1/2+ x, +1/2-y, +1/2+ z
4	C2–H2···Cl1	0.950(3)	2.7631(10)	3.444(4)	129.27(19)	1/2-x, 1+y,1-z
	C5–H5···Cl1	0.951(3)	2.7892(9)	3.705(3)	162.2(2)	1-x, -y,1-z
	C6–H6···Cl1	0.949(3)	2.6997(10)	3.435(4)	134.80(19)	x, y, z
	C14–H14···O1W	0.950(5)	2.588(5)	3.300(8)	132.0(3)	-1/2+x, 2-y, +z
	O15–H15A···O15	0.940(3)	1.771(3)	2.697(7)	167.76(10)	3/2-x, 5/2-y,1/2-z
	O15–H15B···O1W	0.771(3)	1.783(5)	2.527(6)	161.8(3)	x,-1+ y,+ z
	O1W–H 1W1···N8	0.836(5)	2.630(3)	3.151(6)	121.7(3)	1/2+x, 1-y, +z
	O1W–H 1W2···N8	0.840(5)	2.012(3)	2.851(5)	176.9(3)	1/2+x, 2-y, +z
5	C3–H3···O1B	0.949(10)	2.435(7)	3.344(12)	160.15(7)	x, y, z
	C13–H13···O15	0.951(13)	2.525(8)	3.282(14)	136.7(7)	-1/2+x,3/2-y,+z
	C14–H14···O1B	0.951(10)	2.544(7)	3.3234(14)	139.5(7)	x, y, z
	O15–H15···O1B	0.841(7)	1.877(6)	2.709(9)	170.0(6)	1/2+x,3/2-y,1+z
	O1B–H1B···N8	0.839(7)	2.023(8)	2.847(11)	167.1(5)	x, y, z
	C1B–H1B1···O15	0.981(12)	2.486(18)	3.322(15)	143.1(10)	-1+x,+y,-1+z
6	O12–H12···O1A	0.841(7)	1.846(10)	2.684(12)	174.7(6)	1/2+x,1/2-y,2+z
	O1A–H1A···N8	0.837(9)	2.070(9)	2.859(13)	156.9(7)	+x,+y,-1+z
	C14–H14···O1A	0.950(12)	2.607(3)	3.376(1)	138.26	x, y,-1+z
	O1A–H1A···C5	0.837(9)	2.709(2)	3.352(2)	129.12	x, y,-1+z

Table 4. Selected hydrogen bond geometries for coordination compounds **1-6**.

Compounds						
	1	**2**	**3**	**4**	**5**	**6**
π···π	-	-	-	π(N1-C6)-π(N11-C61)[4]	-	-
	-	-	-	dcg-cg= 3.8438(1) dplane-plane= 3.368(1) Doffset= 1.000(18) plane to plane angle= 0.00(19)	-	-
C=N··· π	3.516 and 3.523 3.342 and 3.519[1]	3.417 and 3.559 3.576 and 3.819[2]	3.542 and 3.797 3.379 and 3.565[3]		3.445 and 3.485	3.444 and 3.488
Hg··· π	3.909 4.179	3.950 4.429	3.949 4.376		3.824	3.908

[1]: x,-1+y, z [2]:1+x, y,z [3]: -1+x, y, z [4]: 1/2-x,y,1-z

References

1. B. Moulton and M. J. Zaworotko, *Chemical Reviews*, 2001, **101**, 1629-1658.
2. A. K. Nangia and G. R. Desiraju, *Angewandte Chemie International Edition*, 2019, **58**, 4100-4107.
3. D. Braga, *Journal of the Chemical Society, Dalton Transactions*, 2000, 3705-3713.
4. D. Braga, F. Grepioni, L. Maini and S. d'Agostino, *European Journal of Inorganic Chemistry*, 2018, **2018**, 3597-3605.
5. G. R. Desiraju, *IUCrJ*, 2017, **4**, 710-711.
6. A. M. Beatty, *CrystEngComm*, 2001, **3**, 243-255.
7. J. Reedijk, *Chemical Society Reviews*, 2013, **42**, 1776-1783.
8. T. Hajiashrafi, R. Zekriazadeh, K. J. Flanagan, F. Kia, A. Bauzá, A. Frontera and M. O. Senge, *Acta Crystallographica Section C: Structural Chemistry*, 2019, **75**.
9. C. Janiak, *Journal of the Chemical Society, Dalton Transactions*, 2000, 3885-3896.
10. H. R. Khavasi and A. Azhdari Tehrani, *Inorganic chemistry*, 2013, **52**, 2891-2905.
11. A. A. Tehrani, A. Morsali and M. Kubicki, *Dalton Transactions*, 2015, **44**, 5703-5712.
12. H. Xiang, W.-Y. Gao, D.-C. Zhong, L. Jiang and T.-B. Lu, *CrystEngComm*, 2011, **13**, 5825-5832.
13. H. R. Khavasi and A. A. Tahrani, *CrystEngComm*, 2013, **15**, 5799-5812.
14. S. Wang, Y. Peng, X. Wei, Q. Zhang, D. Wang, J. Dou, D. Li and J. Bai, *CrystEngComm*, 2011, **13**, 5313-5316.
15. S.-S. Hou, X. Huang, J.-G. Guo, S.-R. Zheng, J. Lei, J.-B. Tan, J. Fan and W.-G. Zhang, *CrystEngComm*, 2015, **17**, 947-959.
16. H. R. Khavasi and M. Esmaeili, *CrystEngComm*, 2014, **16**, 8479-8485.
17. W. Wei, H. Yu, F. Jiang, B. Liu, J. Ma and M. Hong, *CrystEngComm*, 2012, **14**, 1693-1700.
18. G. K. Patra, G. Mostafa, D. A. Tocher and D. Datta, *Inorganic Chemistry Communications*, 2000, **3**, 56-58.
19. D. Braga and F. Grepioni, *Accounts of chemical research*, 2000, **33**, 601-608.
20. J. Y. Lu, M. A. Lawandy, J. Li, T. Yuen and C. Lin, *Inorganic Chemistry*, 1999, **38**, 2695-2704.
21. M. Đaković, Ž. Soldin, B.-M. Kukovec, I. Kodrin, C. B. Aakeröy, N. Baus and T. Rinkovec, *IUCrJ*, 2018, **5**, 13-21.
22. L. Brammer, *Chemical Society Reviews*, 2004, **33**, 476-489.
23. C. B. Aakeröy, J. Desper, B. Levin and J. Valdés-Martínez, *Inorganica chimica acta*, 2006, **359**, 1255-1262.
24. T. Hajiashrafi, A. N. Kharat, J. A. Love and B. O. Patrick, *Polyhedron*, 2013, **60**, 30-38.
25. M. Kielmann and M. O. Senge, *Angewandte Chemie International Edition*, 2019, **58**, 418-441.
26. S. Taleghani, M. Mirzaei, H. Eshtiagh-Hosseini and A. Frontera, *Coordination Chemistry Reviews*, 2016, **309**, 84-106.
27. M. T. Kaczmarek, M. Kubicki, A. Mondry, R. Janicki and W. Radecka-Paryzek, *European Journal of Inorganic Chemistry*, 2010, **2010**, 2193-2200.
28. A. Bacchi, M. Carcelli, T. Chiodo, G. Cantoni, C. De Filippo and S. Pipolo, *CrystEngComm*, 2009, **11**, 1433-1441.
29. M. Bruker (2016). APEX3 and SADABS. Bruker AXS Inc., Wisconsin, USA.
30. O. V. Dolomanov, L. J. Bourhis, R. J. Gildea, J. A. Howard and H. Puschmann, *Journal of Applied Crystallography*, 2009, **42**, 339-341.
31. C. P. V. c. Rigaku OD, 2015.
32. G. M. Sheldrick, *Acta Crystallographica Section C: Structural Chemistry*, 2015, **71**, 3-8.
33. a. d. o. U. o. K. a. F. K. G. TURBOMOLE V7.0 2015, 1989-2007, TURBOMOLE GmbH.
34. S. Grimme, *Journal of computational chemistry*, 2006, **27**, 1787-1799.
35. S. F. Boys and F. d. Bernardi, *Molecular Physics*, 1970, **19**, 553-566.
36. J. Contreras-García, E. R. Johnson, S. Keinan, R. Chaudret, J.-P. Piquemal, D. N. Beratan and W. Yang, *Journal of chemical theory and computation*, 2011, **7**, 625-632.
37. E. R. Johnson, S. Keinan, P. Mori-Sanchez, J. Contreras-García, A. J. Cohen and W. Yang, *Journal of the American Chemical Society*, 2010, **132**, 6498-6506.

38. R. C. Gaussian 09, M.J. Frisch, G.W. Trucks, H.B. Schlegel, G.E. Scuseria, M.A. Robb, J.R. Cheeseman, G. Scalmani, V. Barone, G.A. Petersson, H. Nakatsuji, X. Li, M. Caricato, A. Marenich, J. Bloino, B.G. Janesko, R. Gomperts, B. Mennucci, H.P. Hratchian, J.V. Ortiz, A.F. Izmaylov, J.L. Sonnenberg, D. Williams-Young, F. Ding, F. Lipparini, F. Egidi, J. Goings, B. Peng, A. Petrone, T. Henderson, D. Ranasinghe, V.G. Zakrzewski, J. Gao, N. Rega, G. Zheng, W. Liang, M. Hada, M. Ehara, K. Toyota, R. Fukuda, J. Hasegawa, M. Ishida, T. Nakajima, Y. Honda, O. Kitao, H. Nakai, T. Vreven, K. Throssell, J.A. Montgomery, Jr., J.E. Peralta, F. Ogliaro, M. Bearpark, J.J. Heyd, E. Brothers, K.N. Kudin, V.N. Staroverov, T. Keith, R. Kobayashi, J. Normand, K. Raghavachari, A. Rendell, J.C. Burant, S.S. Iyengar, J. Tomasi, M. Cossi, J.M. Millam, M. Klene, C. Adamo, R. Cammi, J.W. Ochterski, R.L. Martin, K. Morokuma, O. Farkas, J.B. Foresman, D.J. Fox, Gaussian, Inc., Wallingford CT, 2016.
39. A. Bacchi, M. Carcelli, T. Chiodo and F. Mezzadri, *CrystEngComm*, 2008, **10**, 1916-1927.
40. A. Bacchi, M. Carcelli, T. Chiodo and P. Pelagatti, *CrystEngComm*, 2010, **12**, 4226-4230.
41. L. Yang, D. R. Powell and R. P. Houser, *Dalton Transactions*, 2007, 955-964.
42. M. A. Spackman and D. Jayatilaka, *CrystEngComm*, 2009, **11**, 19-32.
43. J. B. King, M. R. Haneline, M. Tsunoda and F. P. Gabbaï, *Journal of the American Chemical Society*, 2002, **124**, 9350-9351.
44. J.-Y. Wu, H.-Y. Hsu, C.-C. Chan, Y.-S. Wen, C. Tsai and K.-L. Lu, *Crystal Growth and Design*, 2008, **9**, 258-262.

X1 L. K. Rana, S. Sharma, and G. Hundal, *Crystal Growth and Design*, 2016, **16**, 92-107.

X2 T. S. B. Baul, S. Kundu, S. Mitra, H. Höpfl, E. R. T. Tiekink and A. Linden, *Dalton Trans*., 2013, **42**, 1905-1920.

Graphical Abstract

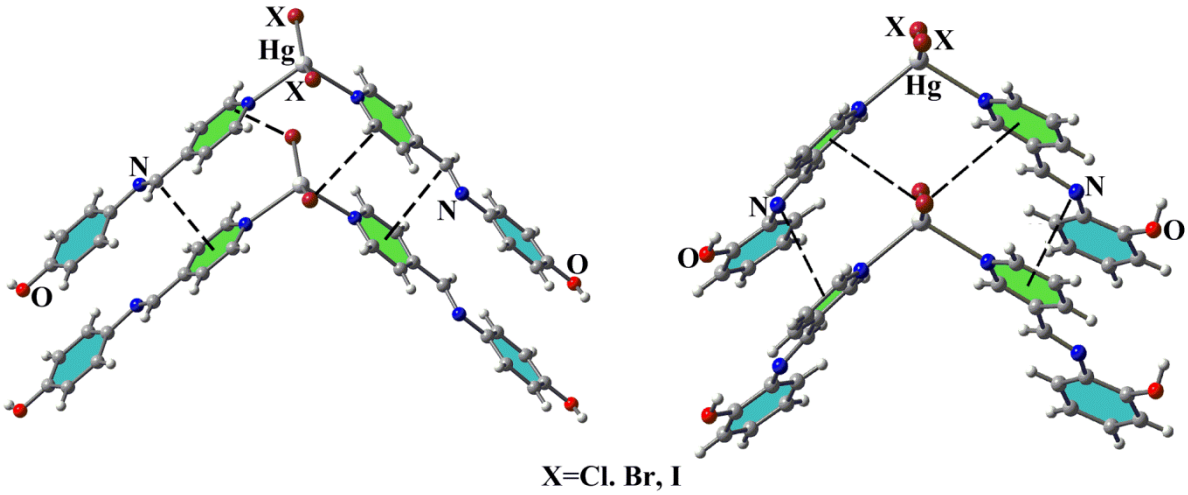

X=Cl. Br, I